Magmatic U-Pb zircon ages west of the Domeyko Fault System, Collahuasi District (Chile): implications for its potential westward continuity

***Cecilia Izquierdo[1,2], Katja Deckart[2], Marcia Muñoz-Gómez[3], Brian Townley[2,4], Yoann Gréau[5,6], Guillermo Fuentes[7,8], Alejandro Sanhueza[9]**

[1]Universidad Arturo Prat, Ingeniería Civil en Minas, Facultad de Ingeniería y Arquitectura, Avda. Arturo Prat 2120, Iquique, Chile.
[2]Universidad de Chile, Departamento de Geología, Plaza Ercilla 803, Santiago, Chile
[3]Universidad Andrés Bello, Geología, Facultad de Ingeniería, República 252, Santiago, Chile.
[4]Centro Avanzado de Tecnología para la Minería (AMTC), Facultad de Ciencias Físicas y Matemáticas, Universidad de Chile, Avda. Tupper 2007, Santiago, Chile
[5] Research School of Earth Sciences, College of Science, The Australian National University, Building 142, Mills Road, Acton, ACT 2601, Australia.
[6] School of Natural Sciences, Faculty of Science and Engineering, Macquarie University, 12 Wally's Walk, Wallumattagal Campus, Macquarie University, NSW 2109, Australia.
[7]Universidad Santo Tomás, Escuela de Geología, Facultad de Ingeniería, Ejército 146, Santiago, Chile.
[8]Consultor Geológica Tect, Santiago, Chile. Eulogía Sánchez 065, Providencia
[9]Compañía Minera Doña Inés de Collahuasi, Baquedano 902, Iquique, Chile.

**Corresponding author (cizquier@unap.cl)*

kdeckart@cec.uchile.cl; *marciamunoz@gmail.com*; *btownley@cec.uchile.cl*; *Yoann.Greau@anu.edu.au*, *Guillermo@tectgeological.com*; *arsanhue@collahuasi.cl*

ABSTRACT

This study presents new high-precision U-Pb zircon age data to document previously unrecognized igneous bodies in a poorly explored sector in the western part of the Collahuasi District, northern Chile. By integrating these new geochronological constraints with detailed geological mapping, petrography, and mineralogical observations, the temporal and spatial patterns of magmatism west of the Domeyko Fault System, the most relevant tectonic structure in the zone, are refined. These patterns reveal multiple magmatic episodes ranging in age from the Permian to the Eocene, some temporally consistent with the Paleocene-early Eocene and late Eocene-early Oligocene metallogenic belts of northern Chile. Of these, the younger event hosts the principal porphyry Cu-Mo deposits of the Collahuasi District, whose distribution is spatially associated with major structures of the Domeyko Fault System.

Keywords: Andean metallogeny, Porphyry copper systems, Paleogene arc activity, Exploration targeting, Metallogenic belts, Central Andes

Edades magmáticas U-Pb en circón al oeste del Sistema de Fallas Domeyko, distrito Collahuasi (Chile): implicancias para su potencial continuidad hacia el oeste. Este estudio presenta nuevos datos de alta precisión de edades U-Pb en circón para documentar cuerpos ígneos previamente no reconocidos en la parte occidental del distrito Collahuasi, norte de Chile, un sector hasta ahora escasamente explorado. Al integrar estas nuevas edades con información geológica, petrográfica y mineralógica de detalle, se provee una actualización de los patrones temporales y espaciales de la actividad magmática al oeste del Sistema de Fallas Domeyko, la estructura tectónica más relevante en la zona. Estos patrones revelan múltiples episodios magmáticos cuyas edades van desde el Pérmico hasta el Eoceno, algunos de ellos correlacionables con las franjas metalogénicas del Paleoceno-Eoceno temprano y del Eoceno tardío-Oligoceno temprano definidas para el norte de Chile. De estos, el evento magmático más joven hospeda los principales depósitos de pórfidos Cu-Mo del distrito Collahuasi, cuya distribución se encuentra espacialmente asociada con las estructuras principales del Sistema de Fallas Domeyko.

Palabras claves: Metalogénesis andina, Sistemas de pórfidos cupríferos, Actividad de arco paleógena, Potencial exploratorio, Franjas metalogénicas, Andes Centrales.

1 Introduction

Northern Chile hosts one of the world's most important concentrations of porphyry copper deposits, including several world-class systems (e.g., Camus and Dilles, 2001; Sillitoe and Perelló, 2005). Together with the deposits of southern Peru, these systems form one of the world's most copper-enriched metallogenic belts (e.g., Mpodozis and Cornejo, 2012). These deposits formed primarily during the Andean tectonic cycle (ongoing since the Jurassic Period), in response to a paleogeographic reorganization of the western margin of Gondwana and the resumption of oceanic subduction (e.g., Richards, 2003; Charrier et al., 2007). During this cycle, the magmatic arc progressively migrated eastward in response to changes in the tectonic configuration of the Andean margin, generating magmatism-related mineral deposits arranged into a series of metallogenic belts parallel to the continental margin and characterized by specific ages (Mpodozis and Ramos, 1990; Richards, 2003; Sillitoe and Perelló, 2005; Mpodozis and Cornejo, 2012) (Fig. 1A). These domains are crossed by a number of tectonic structures, the most relevant being the Domeyko Fault System (DFS) which runs ~N-S along >1,000 km (Maksaev and Zentilli, 1988; Boric et al., 1990; Tomlinson et al., 2001; Ireland, 2010) (Fig. 1A).

The study area is located in the western part of the Eocene-Oligocene Collahuasi District, near 21° S, and encompasses intrusive bodies exposed west of the DFS (Munizaga et al., 2008; Ireland, 2010). In this part of northern Chile, the DFS is commonly referred to as the West Fault System (WFS; Tomlinson et al., 2001; Ireland, 2010). The complex and long-lived tectonic evolution of the West/Domeyko Fault System has been documented along the Domeyko Cordillera (Maksaev, 1990; Berríos and Maksaev, 2015).

In the Collahuasi District, magmatic rocks temporally associated with the Paleocene-early Eocene and late Eocene-early Oligocene metallogenic belts of northern Chile are spatially superimposed, although the principal porphyry Cu-Mo systems of the district formed during the youngest metallogenic event, which includes the world-class Quebrada Blanca, Rosario, and Ujina deposits, as well as the lower-grade, Mo-rich Copaquire system (Maksaev, 1990; Masterman et al., 2004; Maksaev et al., 2007; Ireland, 2010) (Fig. 1A).

While the intrusions associated with the main mineral deposits of the Collahuasi District have been extensively studied (Vergara and Thomas, 1984; Tomlinson et al., 2001; Masterman, 2003; Ireland, 2010; Aguilef et al., 2019), these investigations have largely focused on well-known, presently mined porphyry deposits east of the DFS. That is, intrusive bodies located immediately west of the DFS have so far received little attention in spite of their potential significance for understanding the magmatic and tectonic evolution of the district. In this western domain, the only recognized exploration prospect corresponds to the Copaquire porphyry copper deposit, whose hosting body lacks any detailed relevant studies. Available radiometric age data indicate that Copaquire falls in the Eocene-Oligocene, so it would be coeval with the magmatic episode that characterizes the district as a whole. This asymmetry in geological knowledge hinders a deeper understanding of the tectono-magmatic processes that controlled the distribution and fertility of porphyry-type systems in northern Chile.

The main objective of this contribution is to characterize the petrography, mineralogy, and geochronology of a series of hypabyssal stocks and plutons emplaced west of the Collahuasi District, in order to reconstruct their intrusive history as part of the Paleogene magmatic evolution of the northern Chilean margin. The new data presented here reveal different magmatic events, corresponding to the Paleocene-early Eocene and late Eocene-early Oligocene regional metallogenic belts. This characterization expects to provide valuable base information for future studies west of the DFS.

2 Collahuasi District and Paleogene metallogenic belts

2.1 Antecedents

The Collahuasi District is part of the late Eocene-early Oligocene metallogenic belt of northern Chile, spanning a period between ~45 and 31 Ma (Mpodozis and Cornejo, 2012). This belt extends for approximately 1,400 km along the Domeyko Cordillera, from southern Peru to ~31° S in Chile, in a ~N-S oriented strip that varies in width from 130 km in southern Peru to 30-50 km in northern Chile (García et al., 2017) (Fig. 1A). It is one of the most important metallogenic provinces in the world, hosting the largest copper resources globally, typically present as clusters of two or more Cu-Mo, Cu-Au, or Cu-Mo-Au porphyry-type deposits associated with large plutonic complexes (Sillitoe, 2010; Camus, 2005; Camus and Castelli, 2021) (Fig. 1C). In this context, the deposits of the Collahuasi District: Quebrada

Blanca, Rosario, Ujina, and Copaquire, display a broadly consistent geochronological framework (Masterman et al., 2004; Maksaev et al., 2007, 2009; Ireland, 2010) (Fig. 1B). The published geochronological ages for the main porphyry deposits of the Collahuasi District range from 35.2 to 32.6 Ma (Table 1). These data reinforce the temporal coherence of the Collahuasi District with the metallogenic peak of the belt, within a province that comprises at least 36 deposits and prospects containing ~410 Mt of fine Cu and ~8 Mt of Mo (Camus and Castelli, 2021).

Table 1. Summary of published geochronological ages for the main igneous and hydrothermal events of the Collahuasi District (Rosario, Ujina, and Quebrada Blanca).

Deposit	Geological event	Method	Material	Age±2σ (Ma)	References
Rosario	Hydrothermal biotite alteration of the host andesite.	K-Ar	Secondary biotite	34.2±1.5	Munchmeyer et al. (1984)
	Early-stage potassic alteration associated with A veins.	$^{40}Ar/^{39}Ar$	Secondary biotite	32.9±0.5	Clark et al. (1998)
	Late-stage phyllic alteration associated with TES veins.	$^{40}Ar/^{39}Ar$	Muscovite	32.9±0.6	Clark et al. (1998)
	Cooling/resetting of primary biotite during the early hydrothermal event.	$^{40}Ar/^{39}Ar$	Primary biotite	34.4±0.3	Masterman et al. (2004)
	Crystallization of the Rosario Porphyry.	U-Pb	Zircon	34.2±0.8	Ireland (2010)
	Intermediate-stage illitic alteration associated with C-stage veins.	$^{40}Ar/^{39}Ar$	Illite	34.5±0.5	Masterman et al. (2004)
	Late-stage advanced argillic alteration associated with E-stage veins.	$^{40}Ar/^{39}Ar$	Alunite	32.6±0.3	Masterman et al. (2004)
Ujina	Cooling/resetting of primary biotite, possibly recording hydrothermal alteration of the Ujina Porphyry.	$^{40}Ar/^{39}Ar$	Primary biotite	35.2±0.3	Masterman et al. (2004)
	Crystallization of the largely post-mineral Inca Porphyry.	U-Pb	Zircon	34.4±0.7	Ireland (2010)

Quebrada Blanca	Late hydrothermal event recorded by secondary biotite in the potassic-altered porphyry.	$^{40}Ar/^{39}Ar$	Secondary biotite	34.9±0.4	Maksaev (1990)

The late Eocene-early Oligocene metallogenic belt has also been documented west of the DFS; however, the presence of intrusive bodies of Paleocene age makes it necessary to reconsider a transition zone overprinted by the Paleocene-early Eocene metallogenic belt. This latter belt, which spans in age from ~68 to 51 Ma, extends for more than 1,500 km from southern Peru (~16°20' S) to north-central Chile (~29°30' S) (Fig. 1A). It hosts economically significant deposits in both countries. In fact, according to Camus and Castelli (2021), at least 16 porphyry-type deposits and prospects have been identified between Chile and Peru, collectively containing around 63 Mt of fine copper, of which ~24 Mt are in Chilean territory. Williams (1992) highlighted a spatial segmentation in Paleocene mineralization, with porphyry copper deposits being common in southern Peru and the far north of Chile, and vein-type copper deposits with high concentrations of precious metals (e.g., Au, Ag) more common in the southern (Chilean) portion of the belt, particularly in the Antofagasta Region. The intrusive complexes associated with porphyry systems of the late Eocene-early Oligocene belt were emplaced over a time span of approximately 14 Myr, reflecting a prolonged and episodic magmatic evolution (Camus and Castelli, 2021). Within this evolution, three main stages of porphyry copper deposit formation have been identified (Fig. 1C): an early stage (45-41 Ma), an intermediate stage (39-36 Ma), and a late stage (34-31 Ma), each of which saw the emplacement of at least one giant deposit (>10 Mt of fine copper). A progressive increase in Cu and Mo grades and tonnages is also documented across these stages (Camus and Castelli, 2021) (Fig. 1C). Importantly, the radiometric ages available for the Collahuasi District (Table 1) place it at the transition between the intermediate and late stages (Fig. 1C). This temporal position is consistent with the regional increase in magmatic fertility and metal endowment observed in the late stage and provides a critical framework for interpreting the magmatic and metallogenic evolution of the district, particularly considering the new geochronological constraints presented here.

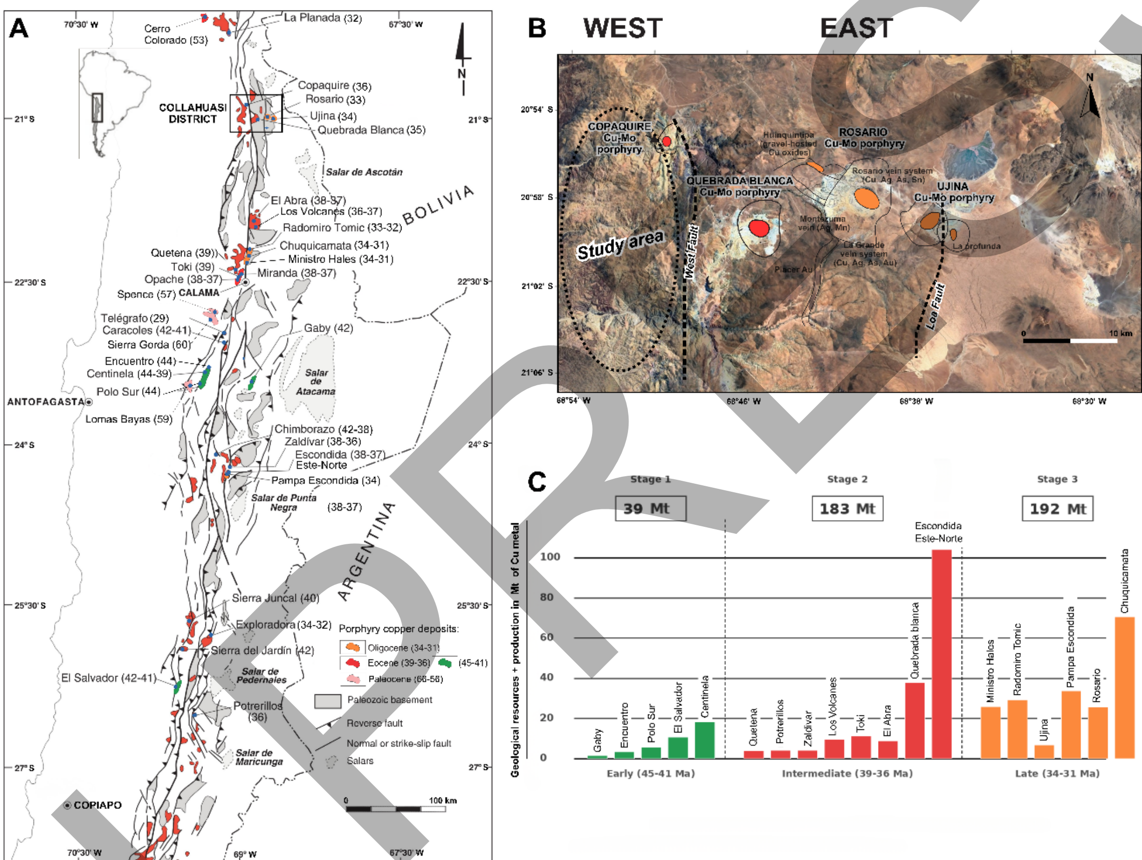

Fig. 1. A. Geological-structural map of northern Chile and adjacent areas, showing the distribution of porphyry copper deposits and the main trace of the Domeyko Fault System (DFS). Paleocene and Eocene porphyry copper deposits, representing both the Paleocene-early Eocene and the late Eocene-early Oligocene metallogenic belts are highlighted (numbers in brackets are in Ma). Map modified from Mpodozis and Cornejo (2012), based on the 1:1,000,000-scale geological map of Chile (Sernageomin, 2002). **B.** Satellite image showing the location of porphyry copper deposits in the Collahuasi District area (rectangle in panel A), including the major centers Rosario, Ujina, Quebrada Blanca, and Copaquire.

Figure modified from Masterman et al. (2004) and Ireland (2009). **C.** Distribution of copper endowment (in Mt of Cu) in porphyry copper deposits formed during the early (45-41 Ma), intermediate (39-36 Ma), and late (34-31 Ma) stages of the late Eocene-early Oligocene metallogenic belt. Figure modified from Camus and Castelli (2021).

2.2 Geological context, intrusive units and prior geochronology

According to previous regional tectonic interpretations (e.g., Maksaev, 1990; Tomlinson et al., 2001), the Collahuasi District can be divided into three W-E main structural blocks (Fig. 2). These domains are separated by major fault systems and display distinct lithological assemblages and tectonic evolutions. From west to east, they are (Fig. 2):

Lomas de Paguana Block: This block comprises units ranging from the Silurian to the Eocene and is structurally dominated by continuous reverse faults with km-scale displacements. The Quehuita Formation (Jurassic-Cretaceous) is the most prominent outcrop, lying unconformably beneath the Cerro Empexa Formation (Cretaceous), with both forming parts of a fold-and-thrust belt. These sequences are intruded by Eocene magmatic bodies. In the southeastern part of the block, the Sierra de Moreno Metamorphic Complex (lower Paleozoic) lies above by means of a thrust fault over the Quehuita Formation (Fig. 2).

Sierra del Medio Block: This uplifted block is dominated by Carboniferous to Permian volcanic and sedimentary rocks of the Collahuasi Formation, together with plutonic and hypabyssal intrusive bodies of Carboniferous, Permian, and Triassic age. It is bounded to the west by the Lomas de Paguana Block across the DFS and to the east by the Eastern Volcanic Chain Block along the El Loa Fault (Fig. 2).

Eastern Volcanic Chain Block: This block is composed mainly of Neogene volcanic rocks, including stratovolcanoes, and is characterized by limited tectonic deformation. Its western boundary with the Sierra del Medio Block is defined by the El Loa Fault (Fig. 2).

The three structural blocks record a common regional evolution, although this evolution is expressed differently within each domain. It can be broadly divided into Paleozoic, Cretaceous, and Eocene stages based on lithological, magmatic, and structural criteria. Figure 2 provides a regional geological and geochronological overview of the Collahuasi District and includes previously published ages from both sides of the DFS. In contrast, Table 2 compiles only the previously published ages from the Lomas de Paguana Block, west of the DFS.

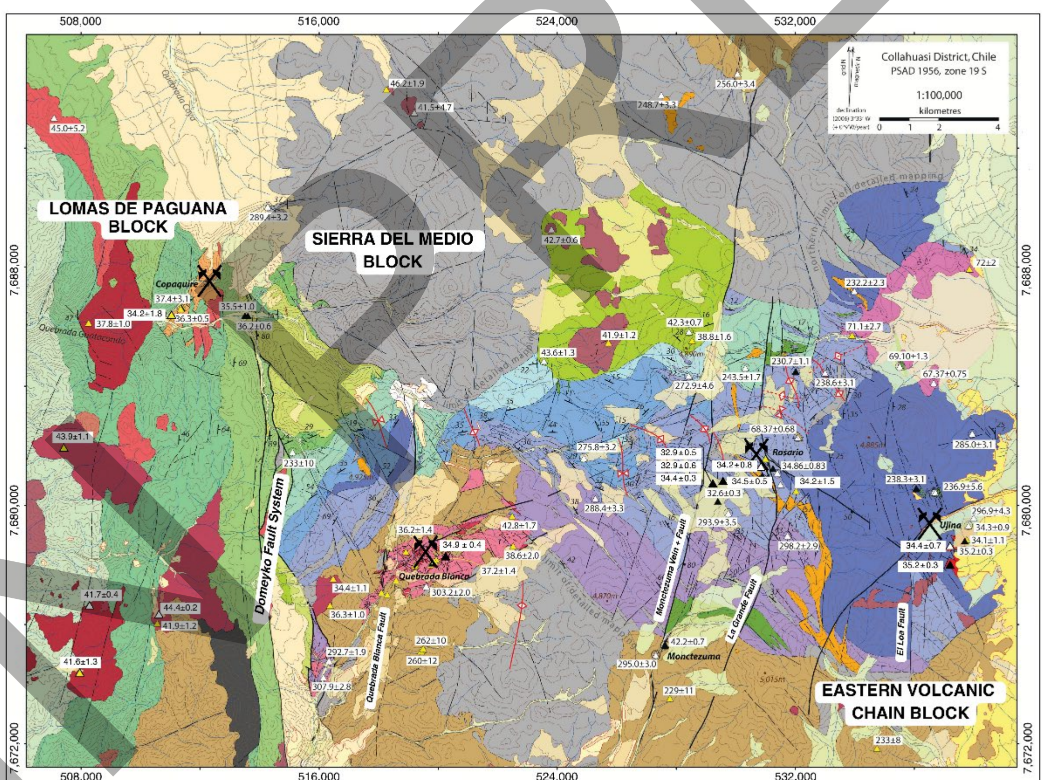

Fig. 2. Geological map of the Collahuasi District area, modified from Ireland (2010) and based on the regional structural framework defined by Maksaev (1990) and Tomlinson et al. (2001). Published geochronological ages for the main porphyry deposits and regional igneous units are also shown; ages for Quebrada Blanca, Rosario, and Ujina are summarized from Table 1.

Table 2. Summary of previously published geochronological data for igneous and hydrothermal events in the study area west of the Domeyko Fault System.

Sample	Location (UTM 19S)	Rock unit	Rock type	Lithology	Method	Mineral	Age±2σ (Ma)	Reference
FT-67	511,410E-7,686,120N	Copaquire Porphyry	Subvolcanic	Granodioritic porphyry	K-Ar	Biotite	34.2±1.8	Boric *et al*. (1990)
FT-67	511,410E-7,686,120N	Copaquire Porphyry	Subvolcanic	Granodioritic porphyry	K-Ar	Biotite	37.4±3.1	Boric *et al*. (1990)
FT-67	511,410E-7,686,120N	Copaquire Porphyry	Subvolcanic	Granodioritic porphyry	$^{40}Ar/^{39}Ar$	Biotite	36.3±0.5	Maksaev (1990)
QBT-47	509,271E-7,685,531N	Pitoguallaca Granodiorite	Plutonic	Granodiorite	K-Ar	Biotite	37.8±1.0	Tomlinson *et al.* (2001)
*QBB-507	504,302E-7,694,520N	Quitala Diorite	Plutonic	Diorite	K-Ar	Biotite	41.7±1.2	Tomlinson *et al.* (2001)
D-7	507,165E-7,692,526N	Quitala Diorite	Plutonic	Diorite	U-Pb	Zircon	45.0±5.2	Vergara and Thomas (1984)
ACO560	507,296E-7,683,293N	Tetas de Copaquire Porphyry	Subvolcanic	Dacitic porphyry	K-Ar	Biotite	43.9±1.1	Aurum (2009)
ACO588	505,462E-7,677,506N	Paguana Quartz monzodiorite	Plutonic	Quartz monzodioritic - dioritic	U-Pb	Zircon	41.7±0.4	Aurum (2009)
DAT-QB-102	507,322E-7,675,261N	Paguana Quartz monzodiorite	Plutonic	Quartz monzodioritic - dioritic	K-Ar	Biotite	41.6±1.3	Tomlinson *et al.* (2001)
QBB-541	510,791E-7,675,811N	Camaruno Granodiorite	Plutonic	Granodiorite	K-Ar	Biotite	41.9±1.2	Tomlinson *et al.* (2001)
QYH-089	510,921E-7,675,817N	Camaruno Granodiorite	Plutonic	Granodiorite	U-Pb	Zircon	44.4±0.2	Aguilef *et al*. (2019)
*PCO1126	507,991E-7,668,134N	Chojas Porphyry	Subvolcanic	Rhyodacitic porphyry	U-Pb	Zircon	51.2±0.6	Aurum (2009)
*QBB-521	507,872E-7,667,381N	Chojas Porphyry	Subvolcanic	Rhyodacitic porphyry	K-Ar	Plagioclase	50.3±2.1	Tomlinson *et al.* (2001)
*DAT-QB-122	507,872E-7,669,291N	Chojas Porphyry	Subvolcanic	Rhyodacitic porphyry	U-Pb	Zircon	43.4±0.7	Damm *et al*. (1990)
*QT-311	510,931E-7,662,562N	Pequetora Granodiorite	Plutonic	Granodiorite	K-Ar	Biotite	42.9±1.2	Tomlinson *et al.* (2001)

Note: Samples marked with an asterisk (*) fall outside the map area defined by Ireland (2010).

3 Methods

A set of representative samples were taken from each of the intrusive bodies without published age data along the western part of the Collahuasi District. The samples (thin and polished sections) were petrographically examined for zircon content prior to U-Pb dating. Eleven samples were thus selected (see Table 3 for microscopic descriptions). Mineral separation was performed at the JV Circones y Minerales SpA (Santiago, Chile) facilities by standard crushing (2 kg of rock sample), heavy liquids, and paramagnetic procedures. Zircon crystals were handpicked under binocular lens and sent to Macquarie GeoAnalytical laboratory, Department of Earth and Environmental Sciences, Macquarie University (Sydney, Australia). The crystals were placed on a double-faced sticky tape and sealed into 1-inch epoxy resin pucks. These pucks were subsequently polished on a polishing lap with a 0.25 µm surface finish. Zircon inspection and cathodoluminescence images were undertaken by a Zeiss EVO MA 15 Scanning Electron Microscope.

Radiometric U-Pb dating in zircon was also carried out at the Macquarie GeoAnalytical laboratory. U-Pb analyses were obtained by utilizing a Photon Machines Analyte Excite 193 nm Excimer equipped with a HelEx II ablation chamber and connected to an Agilent 7700x ICP-MS. A laser spot of 40 µm in diameter was used by default, except for sample C026 which was 35 µm. The carrier gas was helium, and the laser repetition rate was at 5 Hz. Analyses were undertaken with 60 s of background followed by 120 s of ablation. Measured masses were ^{204}Pb, ^{206}Pb, ^{207}Pb, ^{208}Pb, ^{232}Th, and ^{238}U. The zircon GJ-1 (Jackson et al., 2004) was used as primary calibration reference material, and zircons 91500 (Wiedenbeck et al., 1995), Mud Tank (Black and Gulson, 1978; Gain et al., 2019), and Temora 2 (Black et al.,

2003) used as secondary reference materials to monitor the in-run instrument accuracy. Data reduction was performed using the Glitter® software (Griffin, 2008), and all isotopic ratios and ages were corrected for instrumental drift and mass fractionation using the reference zircon GJ-1. Common lead (Pb) corrections were applied only to the calculated ages, using the ComPbCorr Excel template (Anderson, 2002), based on the ^{204}Pb signal. Between 29 and 64 grains were analyzed from each sample to characterize the age variation.

The Microsoft Excel add-in Isoplot (Ludwig, 2009) was used for graphical representations, including frequency distribution histograms, and for age calculations. Uncertainties for individual isotopic ratios and single-spot U-Pb ages reported in the Supplementary File are quoted at the 1σ level, whereas the weighted mean ^{206}Pb/^{238}U ages reported in the text and Table 3 are quoted at the 95% confidence level (2σ). Analyses were evaluated considering concordance, analytical uncertainty, and statistical coherence within the principal zircon age population, following the recommendations of Spencer et al. (2016). The frequency histograms presented here display only the analyses used to calculate the weighted mean age of each sample; inherited zircon populations are not shown. IsoplotR (Vermeesch, 2018) was used to generate Tera–Wasserburg concordia diagrams (Tera and Wasserburg, 1972) and weighted mean plots for samples in which the representative younger population comprised fewer analyses. In total, the eleven samples and their respective diagrams display either a single dominant age population or, where multiple populations are present, the population interpreted to represent crystallization (see Table 3 for a summary of the new age data and the Supplementary File for the complete analytical dataset).

4 New petrographic and U-Pb age data for the western part of the Collahuasi District

As a result of this study, a new geological map was produced for the western part of the Collahuasi District (Fig. 3). This map integrates new field and age information with previously published cartography (Vergara, 1978; Tomlinson et al., 2001; Aguilef et al., 2019). The most relevant units are described following chronological order, from the oldest to the youngest magmatic events.

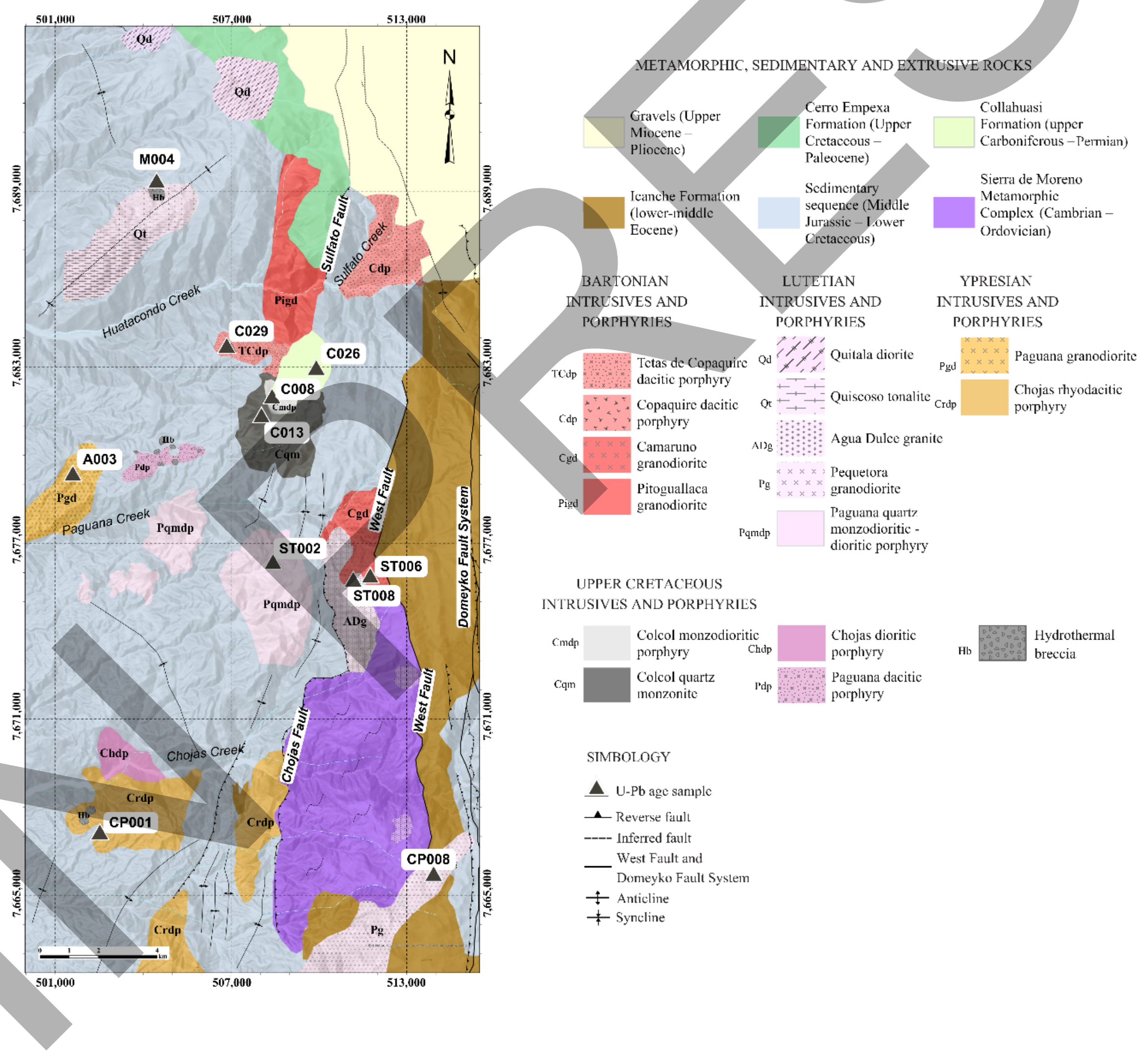

Fig. 3. New geological map of the western sector of the Collahuasi District. The study area encompasses the westernmost part of the map shown in figure 2, in the Lomas de Paguana structural block.

Late Carboniferous to Permian

The Collahuasi Formation is represented by a subvolcanic porphyritic andesite which outcrops at the center of the study area (sample C026). This andesite has serial texture, characterized by tabular plagioclase phenocrysts set in an aphanitic groundmass. The groundmass is composed mainly of plagioclase microlites, accompanied by secondary quartz, biotite, chlorite, and clay minerals (Fig 4A; Table 3). Hydrothermal alteration is moderate and pervasive, affecting approximately one-third of the rock volume, and is expressed by the replacement of feldspars and mafic minerals by secondary biotite, chlorite, clay minerals, quartz, epidote, and minor muscovite. The rock displays veinlets of variable thicknesses and irregular margins, composed predominantly of radial aggregates of epidote and fine-grained quartz, which cut the groundmass and locally replace primary minerals (Fig. 4B; Table 3).

Zircon grains from this andesite rock sample yield a weighted mean $^{206}Pb/^{238}U$ age of 269.3±2.7 Ma (MSWD=1.3), calculated using the three youngest concordant analyses. The remaining zircon analyses define significantly older age populations, extending up to ca. 2000 Ma, and are interpreted as inherited components, being therefore excluded from the age calculation. The youngest zircon population is interpreted to record the crystallization age of the intrusive body, supporting its assignment to the Collahuasi Formation of late Carboniferous-Permian age (Fig. 4C-E).

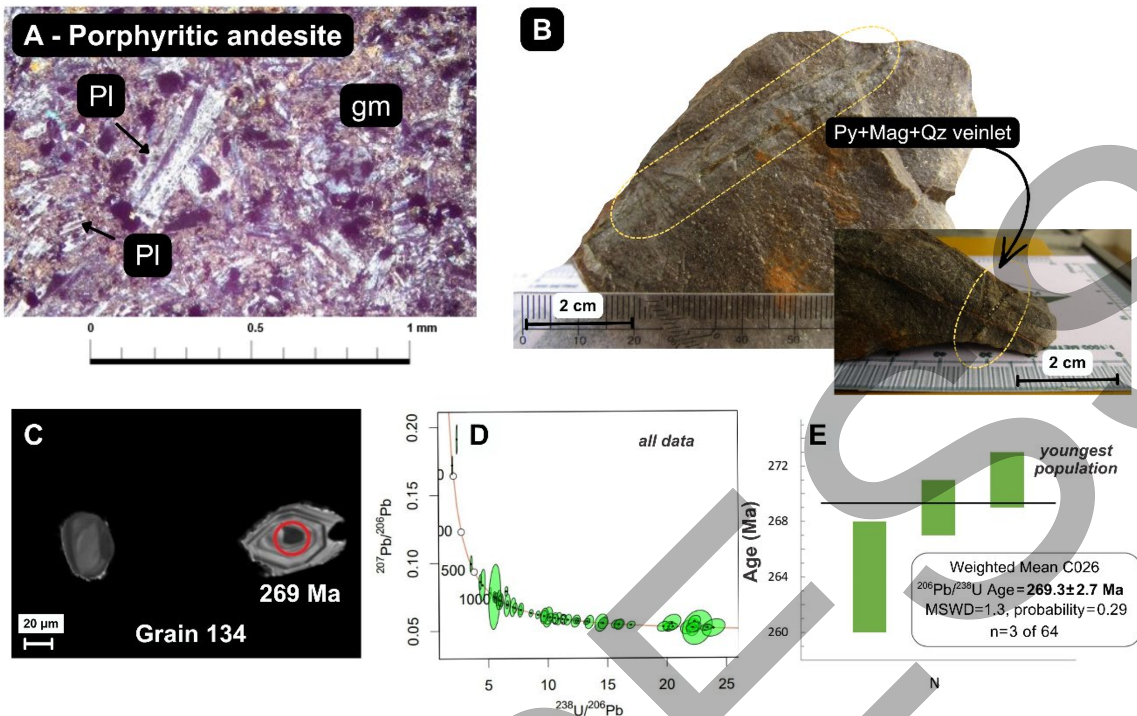

Fig. 4. Petrographic and geochronological results for sample C026. **A.** Photomicrograph of a subvolcanic porphyritic andesite under crossed polarized light (XPL, 20×). **B**. Hand specimen of the andesitic body with an opaque mineral-filled veinlet. **C.** Representative cathodoluminescence image of zircon grains. **D.** Tera-Wasserburg concordia diagram. **E.** Age bar graph, with box heights at 1σ and weighted mean indicated by the horizontal black line. Pl: plagioclase; gm: groundmass; Py: pyrite; Mag: magnetite; Qz: quartz. See Supplementary File for details.

Late Cretaceous (Maastrichtian)

Two intrusive igneous bodies of Late Cretaceous age are recognized in the central sector of the study area, bounded to the north by the Huatacondo creek and to the south by the Paguana creek: a plutonic quartz monzonite (Cqm; sample C013) and a subvolcanic monzodioritic porphyry (Cmdp; sample C008), hereafter collectively referred to as the Colcol intrusive suite. Both intrusions are characterized by intermediate compositions dominated by plagioclase, K-feldspar, quartz, and mafic minerals, and display moderate to intense, pervasive hydrothermal alterations expressed by propylitic to sericitic assemblages that replace feldspars and mafic phases (Fig. 5A, B, F, G; Table 3).

Based on concordant zircon populations, U-Pb dating indicates a weighted mean $^{206}Pb/^{238}U$ age of 67.1±0.4 Ma (MSWD=1.2) for sample C013, and a weighted mean $^{206}Pb/^{238}U$ age of 66.6±0.5 Ma (MSWD=0.92) for sample C008 (Fig. 5D, E, I, J). These ages constrain the emplacement of the Colcol intrusive suite to the Maastrichtian.

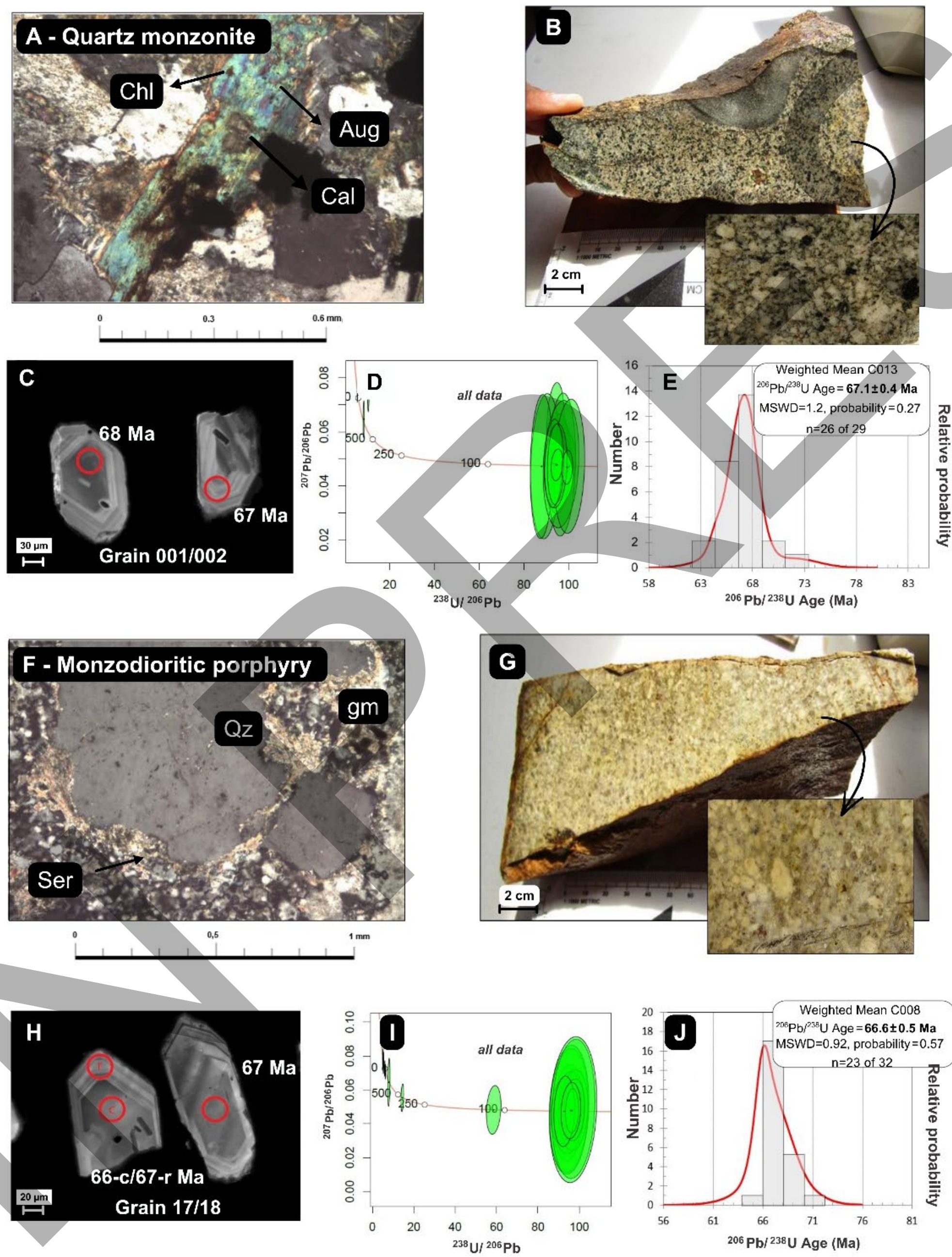

Fig. 5. Petrographic and geochronological results for samples C013 (A-E) and C008 (F-J). **A.** Photomicrograph of a quartz monzonite under crossed polarized light (XPL, 100×). **B.** Hand specimen of

the quartz monzonite showing a plutonic texture. **C.** Representative cathodoluminescence image of zircon grains. **D.** Tera-Wasserburg concordia diagram. **E.** Cumulative probability curve and frequency histogram for points included in the age calculation. **F.** Photomicrograph of a monzodioritic porphyry under crossed polarized light (XPL, 50×). **G.** Hand specimen of the monzodioritic porphyry showcasing its porphyritic texture. **H.** Representative cathodoluminescence image of zircon grains. **I.** Tera-Wasserburg concordia diagram. **J.** Cumulative probability curve and frequency histogram for points included in the age calculation. Chl: chlorite; aug: augite; gm: groundmass; Qz: quartz; Ser: sericite. See Supplementary File for details.

<u>Early Eocene (Ypresian)</u>

Two intrusive to subvolcanic igneous bodies of early Eocene age are recognized in the study area: the Paguana granodiorite (Pgd; sample A003) and the Chojas rhyodacitic porphyry (Crdp; sample CP001). The Pgd unit forms a relatively isolated body in the central-western part of the study area, whereas Crdp has a broader distribution and is exposed throughout the southern sector (Fig. 3). These units display felsic to intermediate compositions dominated by plagioclase and quartz, with subordinate K-feldspar and biotite, and record variable degrees of hydrothermal alteration (Fig. 6A, B, F, G; Table 3). Alteration is weak to moderate and pervasive in the granodiorite, mainly expressed by albitization and localized sericitization of plagioclase, whereas the rhyodacitic porphyry is characterized by moderate to intense quartz-sericite alteration overprinted by strong argillic alteration in the groundmass (Fig. 6A, F; Table 3). In sample CP001, sulfide and oxide mineralization is hosted within hydrothermal breccias developed in the southern sector. In sample A003, mineralization is restricted to a vein cutting the granodioritic intrusion.

U-Pb zircon dating constrains the emplacement of these units to the Ypresian. Sample CP001 (Chojas rhyodacitic porphyry) yields a weighted mean $^{206}Pb/^{238}U$ age of 51.0±0.5 Ma (MSWD=0.31), whereas sample A003 (Paguana granodiorite) yields a weighted mean $^{206}Pb/^{238}U$ age of 50.0±0.8 Ma (MSWD=1.3) based on concordant zircon analyses (Fig. 6D, E, I, J). Previously reported U-Pb and K-Ar ages for the rhyodacitic porphyry summarized in Table 2, are consistent with these results.

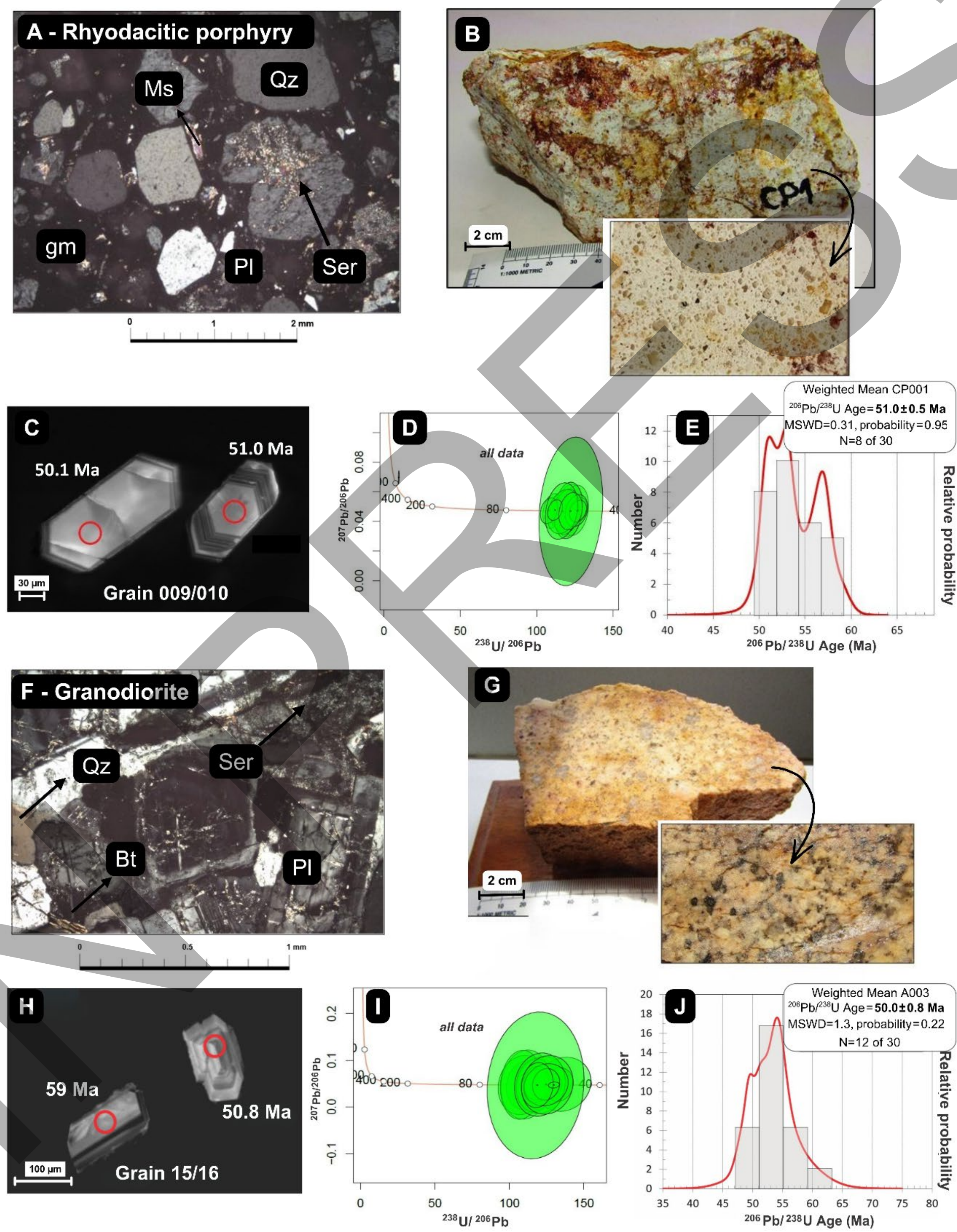

Fig. 6. Petrographic and geochronological results for samples CP001 (A-E) and A003 (F-J). **A.** Photomicrograph of a rhyodacitic porphyry under crossed polarized light (XPL, 20×). **B.** Hand specimen of the rhyodacitic porphyry showcasing its porphyritic texture. **C.** Representative cathodoluminescence image of zircon grains. **D.** Tera-Wasserburg concordia diagram. **E.** Cumulative probability curve and frequency histogram for points included in the age calculation. **F.** Photomicrograph of a granodiorite under crossed polarized light (XPL, 50×). **G.** Hand specimen of the granodiorite displaying its plutonic texture. **H.** Representative cathodoluminescence image of zircon grains. **I.** Tera-Wasserburg concordia diagram. **J.** Cumulative probability curve and frequency histogram for points included in the age calculation. Ms: muscovite; Qz: quartz; Pl: plagioclase; Ser: sericite; gm: groundmass; Bt: biotite. See Supplementary File for details.

Middle Eocene (Lutetian)

Several igneous bodies of early middle Eocene age are recognized in the study area, consisting of tonalites (Qt; sample M004), granodiorites (Pg; sample CP008), and granites (ADg; sample ST008), together with a subvolcanic quartz monzodioritic-dioritic porphyry (Pqmdp; sample ST002). These units form small, discontinuous stocks and porphyry bodies, with individual mapped exposures generally covering less than ~15 km^2. They are distributed across much of the study area, with the Qt unit exposed in the northwestern sector, Pqmdp mainly in the central sector, ADg in the east-central sector, and Pg along the southeastern margin (Fig. 3). These rocks are dominated by plagioclase and quartz, with variable proportions of K-feldspar, amphibole, and biotite, and display medium- to coarse-grained equigranular textures in the plutonic intrusions, contrasting with the porphyritic texture of the quartz monzodiorite-diorite (Figs. 7A, B, F, G and 8A, B, F, G; Table 3). Hydrothermal alteration is generally weak to moderate, ranging from localized sericitic overprinting in the granitic and granodioritic bodies (Figs. 7F and 8A; Table 3) to more developed propylitic assemblages in the tonalite and quartz monzodioritic-dioritic porphyry, characterized by epidote-chlorite-calcite replacement of feldspars and mafic minerals (Figs. 7A and 8F; Table 3).

U-Pb zircon ages indicate that these intrusions were emplaced during the Lutetian (Figs. 7D, E, I, J and 8D, E, I, J). Sample M004 (Quiscoso tonalite) yields a weighted mean $^{206}Pb/^{238}U$ age of 45.4±0.3 Ma (MSWD=0.96), consistent with previously reported ages for nearby tonalitic and quartz dioritic bodies (Table 2). Sample ST002 (Paguana quartz monzodioritic-dioritic porphyry) gives a weighted mean $^{206}Pb/^{238}U$ age of 41.6±0.2 Ma (MSWD=1.4), in agreement with published U-Pb and K-Ar data for this unit (Table 2). Similarly, sample ST008 (Agua Dulce granite) yields a weighted mean $^{206}Pb/^{238}U$ age of 41.7±1.0 Ma (MSWD=1.9; see below), and sample CP008 (Pequetora granodiorite) provides a $^{206}Pb/^{238}U$ age of 42.8±0.3 Ma (MSWD=1.4). Previously published U-Pb and K-Ar ages for these granitic and granodioritic intrusions are summarized in Table 2 and are broadly consistent with the new geochronological results, confirming a main intrusive pulse between ~45 and 42 Ma in the study area.

For sample ST008, two analyses were excluded from the age calculation. The 39.3±0.9 Ma analysis is strongly (80%) discordant and is interpreted to reflect radiogenic Pb loss. Although the analyzed grain contains only minor inclusions, most of the zircon grains in the sample display pervasive fracturing and internal porosity, indicating disturbance of the U-Pb system. A second analysis at 45.3 Ma was excluded because it lies outside the main ~42-40 Ma age cluster and is interpreted as an inherited or antecrystic component. The crystallization age was calculated using only the youngest coherent population of concordant analyses, which define a robust weighted mean age (Fig. 8E).

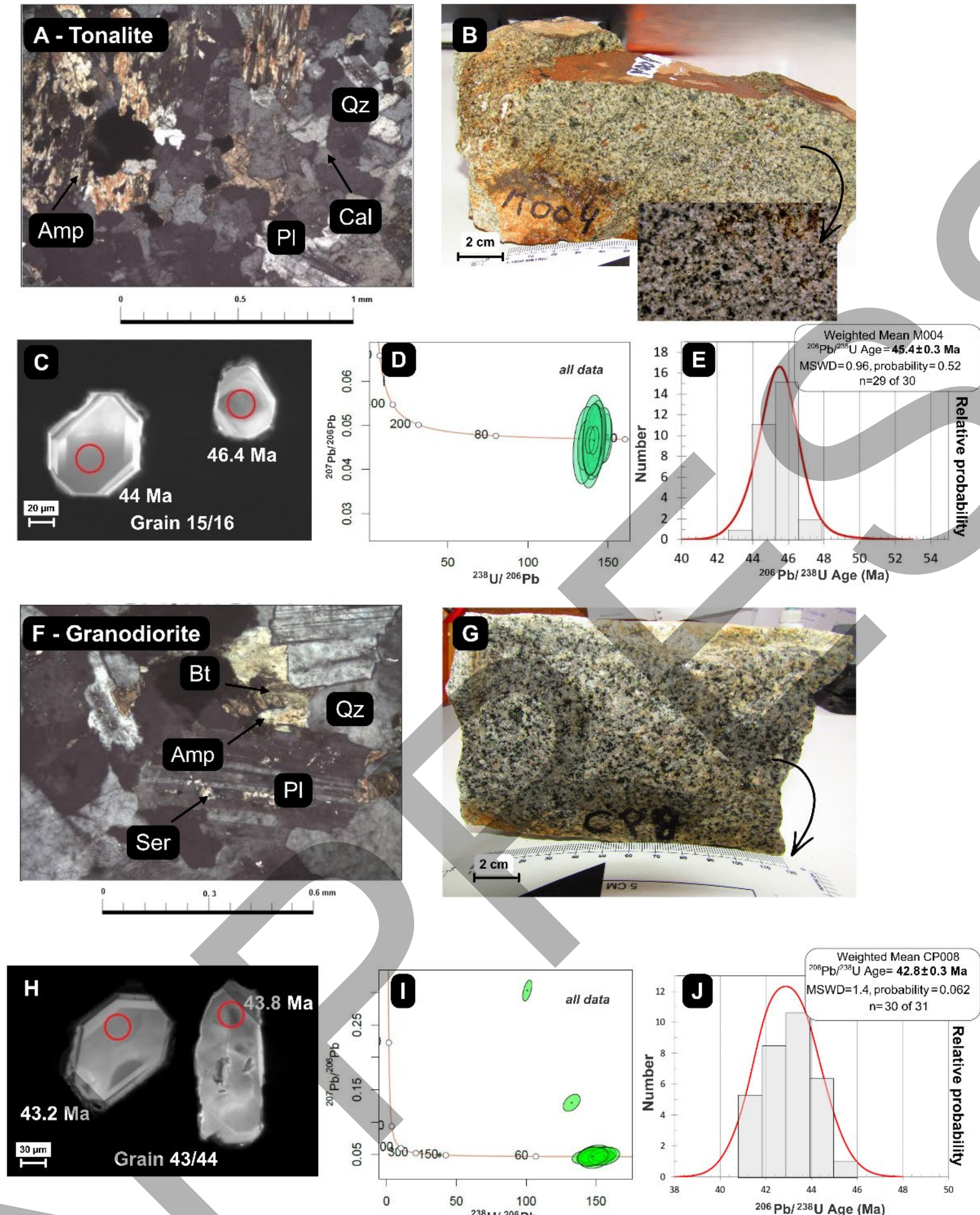

Fig. 7. Petrographic and geochronological results for samples M004 (A-E) and CP008 (F-J). **A.** Photomicrograph of a tonalite under crossed polarized light (XPL, 200×). **B.** Hand specimen of the tonalite showing a plutonic texture. **C.** Representative cathodoluminescence image of zircon grains. **D.** Tera-Wasserburg concordia diagram. **E.** Cumulative probability curve and frequency histogram for points included in the age calculation. **F.** Photomicrograph of a granodiorite under crossed polarized light (XPL, 100×). **G.** Hand specimen of the granodiorite displaying a plutonic texture. **H.** Representative cathodoluminescence image of zircon grains. **I.** Tera-Wasserburg concordia diagram **J.** Cumulative probability curve and frequency histogram for points included in the age calculation. Amp: amphibole; Qz: quartz; Pl: plagioclase; Cal: calcite; Bt: biotite; Ser: sericite. See Supplementary File for details.

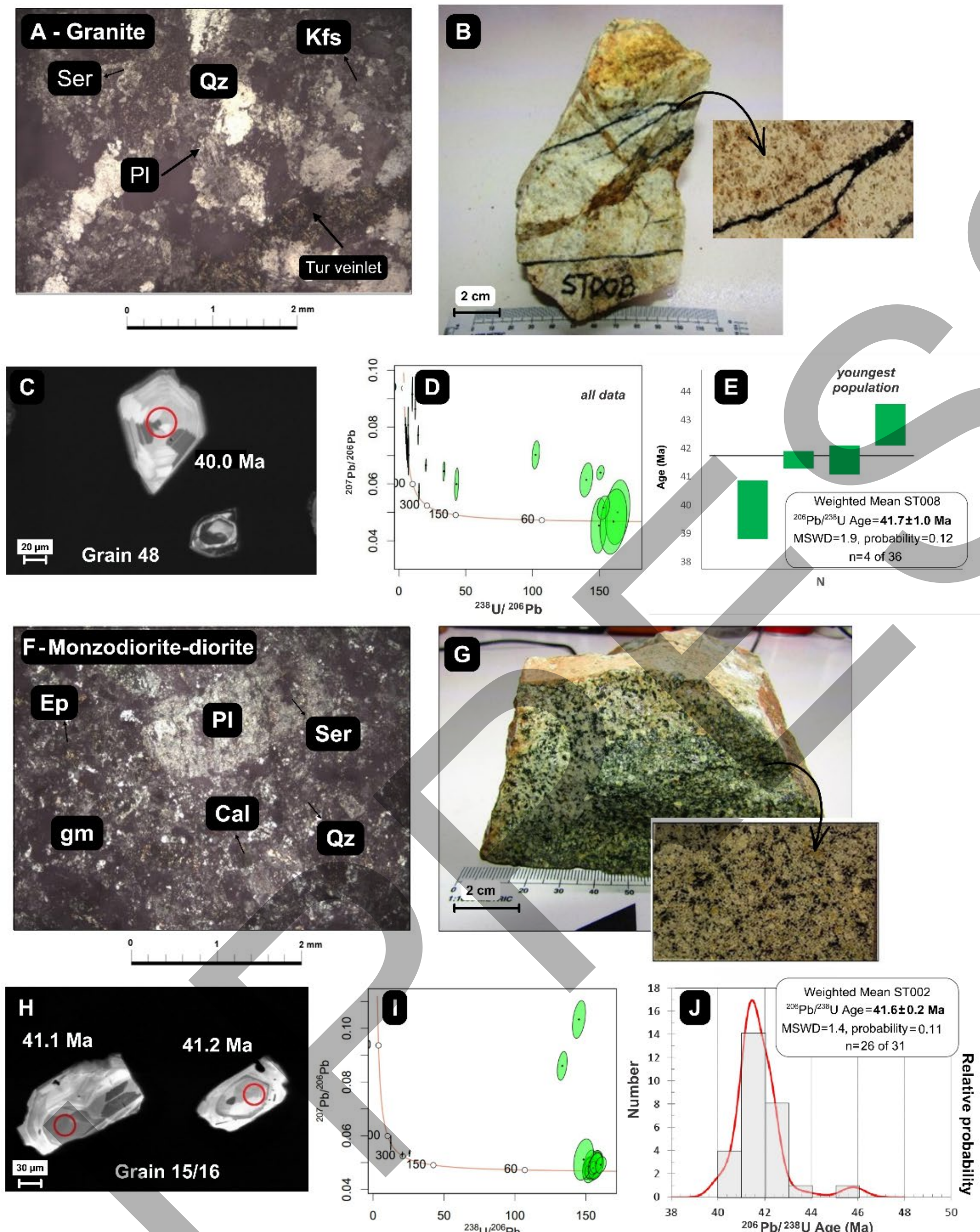

Fig. 8. Petrographic and geochronological results for samples ST008 (A-E) and ST002 (F-J). **A.** Photomicrograph of a granite under crossed polarized light (XPL, 20×) **B.** Hand specimen of the granite body showing a phaneritic plutonic texture. **C.** Representative cathodoluminescence image of zircon grains. **D.** Tera-Wasserburg concordia diagram. **E.** Age bar graph, with box heights at 1σ and weighted mean indicated by the horizontal black line. **F.** Photomicrograph of a quartz monzodioritic-dioritic porphyry under crossed polarized light (XPL, 20×). **G.** Hand specimen of the monzodiorite-diorite body displaying a porphyritic subvolcanic texture. **H.** Representative cathodoluminescence image of zircon grains. **I.** Tera-Wasserburg concordia diagram. **J.** Cumulative probability curve and frequency histogram for points included in the age calculation. Ser: sericite; Qz: quartz; Kfs: K-feldspar; Pl: plagioclase; Tur: tourmaline; Ep: epidote; Cal: Calcite; gm: groundmass. See Supplementary File for details.

Middle Eocene (Bartonian)

Two igneous bodies of late middle Eocene age are recognized in the study area: the Tetas de Copaquire dacitic porphyry (TCdp; sample C029), of subvolcanic character, and the Camaruno granodiorite (Cgd; sample ST006), of plutonic character. These rocks display felsic compositions dominated by plagioclase and quartz, with subordinate biotite, K-feldspar, and amphibole, and exhibit porphyritic and phaneritic textures (Fig. 9A, B, F, G; Table 3). Hydrothermal alteration is moderate and pervasive in the TCdp unit, characterized by sericitic-argillic assemblages affecting feldspars and biotite, whereas the Cgd unit records only weak and localized alteration, mainly expressed by sericitization and a minor propylitic overprint (Fig. 9A, F; Table 3).

U-Pb zircon ages constrain the emplacement of these units to the Bartonian (Fig. 9D, E, I, J). Sample C029 (Tetas de Copaquire dacite porphyry) yields a weighted mean $^{206}Pb/^{238}U$ age of 40.0±0.3 Ma (MSWD=1.7), indicating a slightly younger emplacement than previously reported K-Ar biotite ages for this unit (Table 2). Sample ST006 (Camaruno granodiorite) yields a weighted mean $^{206}Pb/^{238}U$ age of 37.6±0.3 Ma (MSWD=1.5) based on four concordant zircon analyses (Fig. 9J), being younger than previously reported K-Ar and U-Pb ages for the same body (Table 2). Cathodoluminescence images show that the dated zircons from ST006 include both internal and rim domains (Fig. 9H).

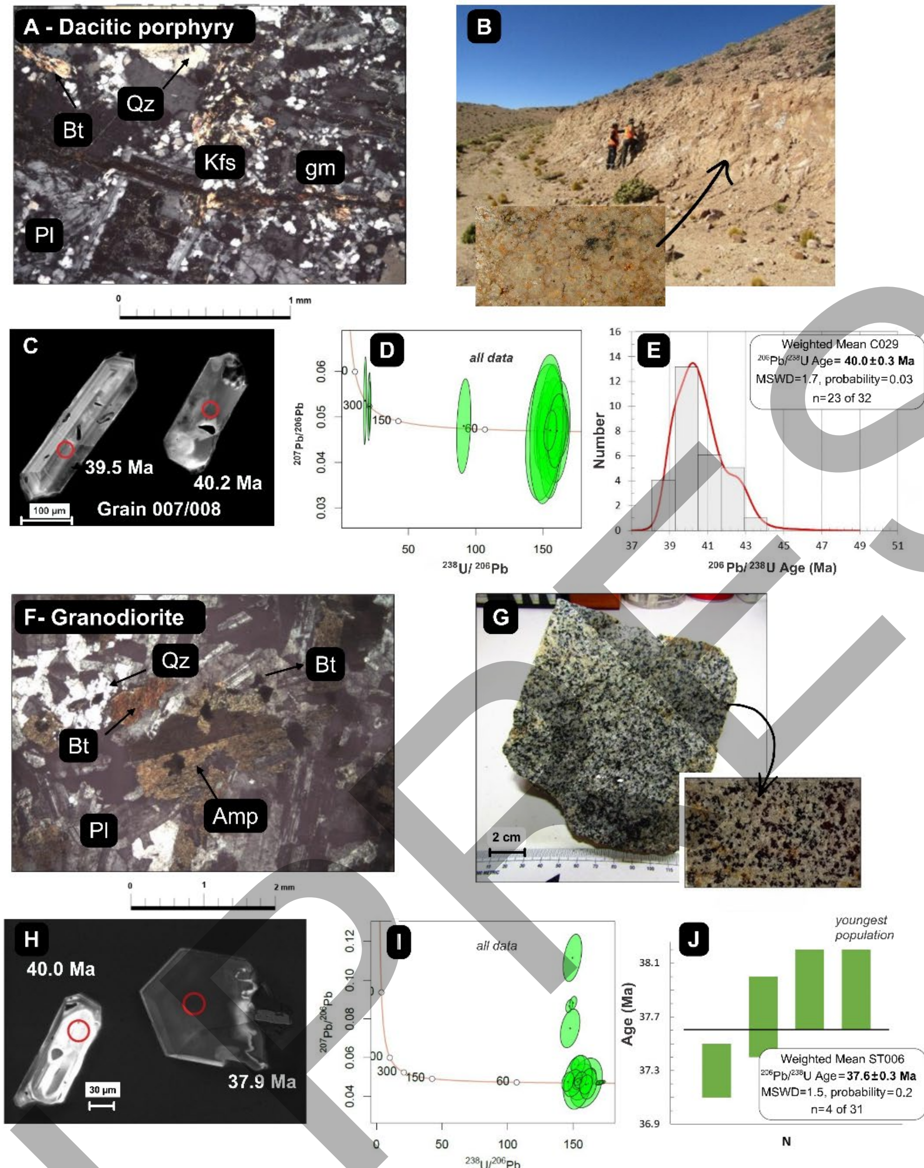

Fig. 9. Petrographic and geochronological results for samples C029 (A-E) and ST006 (F-J). **A.** Photomicrograph of a dacitic porphyry under crossed polarized light (XPL, 50×). **B.** Hand specimen of the dacite displaying a porphyritic subvolcanic texture; an outcrop of the intrusive is also shown. **C.** Representative cathodoluminescence image of zircon grains. **D.** Tera-Wasserburg concordia diagram. **E.** Cumulative probability curve and frequency histogram for points included in the age calculation. **F.** Photomicrograph of a granodiorite under crossed polarized light (XPL, 20×). **G.** Hand specimen of the granodiorite with a phaneritic plutonic texture. **H.** Representative cathodoluminescence image of a zircon grain. **I.** Tera-Wasserburg concordia diagram. **J.** Age bar graph, with box heights at 1σ and weighted mean indicated by the horizontal black line. See Supplementary File for details.

Table 3. Petrographic descriptions of the most representative samples from the study area. See Supplementary File for additional details.

Sample	Rock unit	Location (UTM 19S)	Lithology	Description	Alteration	U-Pb ages (mean±2σ; Ma)
C026	Collahuasi Formation	509,955E-7,682,976N	Andesite	Porphyritic; serial texture; aphanitic groundmass; dominated by plagioclase with subordinate clinopyroxene and minor opaques.	Moderate, pervasive propylitic alteration (chlorite-epidote±calcite), locally overprinted by slight sericitic alteration (sericite-quartz±pyrite).	269.3±2.7
C013	Colcol quartz monzonite	507,993E-7,681,234N	Quartz monzonite	Phaneritic; equigranular texture with plagioclase, K-feldspar, quartz, and pyroxenes±amphibole.	Strong, pervasive propylitic alteration (epidote-chlorite-albite±sericite±calcite).	67.1±0.4
C008	Colcol monzodioritic porphyry	508,663E-7,681,620N	Monzodioritic porphyry	Porphyritic; dominated by plagioclase, K-feldspar, quartz, biotite, and amphibole.	Moderate to intense sericitic-chloritic alteration with albite, epidote, calcite, clays±jarosite and rutile.	66.6±0.5
A003	Paguana granodiorite	501,667E-7,679,359N	Granodiorite, plutonic	Phaneritic; inequigranular texture with plagioclase, quartz, K-feldspar, and biotite.	Slight to moderate albitization and localized sericitization of plagioclase.	50.0±0.8
CP001	Chojas rhyodacitic porphyry	502,655E-7,667,093N	Rhyodacitic porphyry	Porphyritic; seriate texture with quartz and plagioclase phenocrysts in a highly altered matrix.	Moderate to strong quartz-sericite alteration overprinted by strong argillic alteration.	51.0±0.5
M004	Quiscoso tonalite	504,471E-7,689,221N	Tonalite, plutonic	Phaneritic; equigranular with plagioclase, quartz, amphibole, and minor titanite and zircon.	Moderate propylitic alteration dominated by chlorite±clays±calcite.	45.4±0.3
ST002	Paguana quartz monzodioritic-dioritic porphyry	508,532E-7,676,385N	Monzodioritic to dioritic porphyry	Porphyritic; dominated by plagioclase phenocrysts and altered amphibole in a fine- to medium-grained groundmass.	Strong propylitic alteration (epidote-chlorite-calcite±sericite±clays).	41.6±0.2
ST008	Agua Dulce granite	511,346E-7,675,767N	Granite	Phaneritic; equigranular with K-feldspar, quartz, and plagioclase.	Moderate sericitic alteration with minor argillic overprint.	41.7±1.0
CP008	Pequetora granodiorite	513,927E-7,665,673N	Granodiorite, plutonic	Phaneritic; equigranular with plagioclase, quartz, K-feldspar, amphibole, and biotite.	Slight sericitic alteration with minor secondary biotite and clays.	42.8±0.3
C029	Tetas de Copaquire dacite porphyry	507,000E-7,683,700N	Dacitic porphyry	Porphyritic; dominated by plagioclase, biotite, quartz, and minor K-feldspar.	Moderate sericitic-argillic alteration with albite and minor muscovite±jarosite.	40.0±0.3
ST006	Camaruno granodiorite	511,878E-7,675,894N	Granodiorite, plutonic	Phaneritic; inequigranular with plagioclase, quartz, K-feldspar, amphibole, and biotite.	Slight alteration with fine sericite, minor epidote (zoisite), and cryptocrystalline clays.	37.6±0.3

5 Discussion

5.1. Tectono-magmatic context and regional evolution

Within the regional framework of Paleocene-Eocene magmatism in northern Chile, the new geochronological results presented here refine the temporal evolution of intrusive activity west of the DFS. The identification of two distinct Eocene age populations (~45-42 and ~40-38 Ma) suggests that magmatism in the western part of the Collahuasi District was not restricted to a single short-lived intrusive episode but instead occurred through multiple temporally discrete pulses. This pattern is consistent with the episodic nature of Paleogene magmatism recognized along the Domeyko Cordillera and with regional models linking the spatial and temporal evolution of arc magmatism in northern Chile to changes in plate convergence, crustal deformation, and tectonic reorganization (Scheuber et al., 1994; Kay and Mpodozis, 2001; Richards, 2003; Sillitoe and Perelló, 2005).

The occurrence of coeval Eocene magmatism on both sides of the DFS further suggests that this structure did not act as a strict lithospheric boundary limiting magma emplacement. In the study area, the DFS may have functioned as a crustal-scale weakness zone that facilitated magma ascent and localized intrusive activity. Comparable relationships between arc magmatism and major strike-slip fault systems have been documented elsewhere in northern Chile, particularly along the Atacama Fault Zone (Scheuber and Andriessen, 1990).

5.2. New geochronological evidence and tectonic interpretations

The central part of the study area records a wide age range from the Permian (~269 Ma) to the Eocene (~ 38 Ma), reflecting significant structural and stratigraphic complexities. In particular, the Permian age corresponds to a subvolcanic porphyritic andesite (sample C026) assigned to the Collahuasi Formation, whose presence in the study area had not been previously recognized. This new age constraint confirms the westward extension of the Permian volcanic-subvolcanic basement and supports previous interpretations that proposed a late Paleozoic andesitic-dacitic substratum beneath the Collahuasi District (Maksaev, 1990; Tomlinson et al., 2001; Munizaga et al., 2008).

The new U-Pb zircon data obtained here provide additional constraints on the timing of Eocene magmatism in the central portion of the study area. Previously published ages clustered mainly between ~44 and 41 Ma (Table 2) and have been interpreted as recording a single intrusive episode (e.g., Tomlinson et al., 2001; Aguilef et al., 2019). Our new data reveals a more complex temporal pattern. Sample C029 (Tetas de Copaquire dacite porphyry) yields an emplacement age of 40.0±0.3 Ma, overlapping with the younger end of the published range. Similarly, sample ST006 (Camaruno granodiorite) records a crystallization age of 37.6±0.3 Ma and exhibits two distinguishable zircon age populations: an older group overlapping with the ~44-41 Ma age range and a younger population defining the 37.6 Ma age. Comparison between published and new U-Pb ages therefore highlights an Eocene bimodal age distribution, with an older population at ~45-42 Ma and a younger population at ~40-38 Ma, indicating that Eocene magmatism in the central-western part of the Collahuasi District occurred through at least two temporally distinct intrusive pulses rather than as a single event.

5.3. Connection between magmatism and metallogenic potential

The magmatic history of the study area is defined by three main pulses that reflect both basement inheritance and subsequent arc-related magmatism. The first pulse corresponds to a late Permian event (~269 Ma), represented by subvolcanic intrusions of porphyritic andesite assigned to the Collahuasi Formation, which constitute part of the pre-Andean volcanic-subvolcanic basement.

The second pulse comprises Late Cretaceous intrusive activity (~67-66 Ma), represented by the Colcol intrusive suite. Although volumetrically subordinate to the Paleogene magmatism, this event records an early stage of arc-related intrusions in the study area. Comparable Campanian-Maastrichtian intrusive ages have been documented in the Cerro Colorado and Sierra Gorda districts (Vergara and Thomas, 1984; Tomlinson et al., 2001; Masterman, 2003), where Upper Cretaceous intrusions constitute part of the magmatic basement underlying Paleocene-Eocene porphyry systems.

The third and most volumetrically significant pulse corresponds to Paleocene-Eocene magmatism, widely represented by multiple subvolcanic and intrusive bodies distributed from north to south across the study area. These include the Chojas rhyodacitic porphyry (~51 Ma), the Tetas de Copaquire dacitic porphyry (~40 Ma), the Paguana (~50 Ma), Pequetora (~42.8 Ma), and Camaruno (~37.6 Ma) granodiorites, as well as the Paguana monzodioritic-dioritic porphyry (~41.6 Ma), the Agua Dulce granite (~41.7 Ma), and the Quiscoso tonalite (~45.4 Ma). Among these units, the Camaruno granodiorite is particularly relevant, as its emplacement age overlaps with the main mineralization intervals recognized in porphyry copper deposits of the Collahuasi District, such as Rosario and Ujina (Camus and Castelli, 2021; Table 1). Although the Copaquire prospect has not been dated by U-Pb, a biotite $^{40}Ar/^{39}Ar$ age of 36.3±0.5 Ma (Maksaev, 1990; Table 2), possibly recording hydrothermal alteration, provides additional evidence for the metallogenic potential of this western block. Furthermore, the lithological assemblage recognized in the study area is equivalent to that reported from the main mineralized centers of the Collahuasi District. The spatial superposition of late Paleozoic basement rocks and Paleogene intrusive activity is also consistent with the recurrent localization of Cenozoic porphyry Cu systems within older magmatic domains documented elsewhere in the Central Andes (Sillitoe and Perelló, 2024). This convergence in age, intrusive style, and evidence of hydrothermal activity supports the interpretation of a probable westward extension of the Collahuasi magmatic-metallogenic system. In this context, the Colcol and Chojas sectors warrant further investigations to assess their potential relationship with the Paleogene magmatic and metallogenic evolution of the Collahuasi District.

The temporal relationships between the magmatic pulses identified in this study and the main metallogenic stages of Camus and Castelli (2021) are summarized in figure 10. This diagram illustrates the long-lived magmatic evolution of the western block, from a late Permian (Roadian) basement age to Paleogene arc-related intrusions and highlights the temporal overlap between the Paleocene-Eocene intrusive bodies dated in this study and the early to intermediate metallogenic stages (Fig. 1C). This temporal coincidence points to a magmatic development west of the West Fault contemporaneous with the main mineralizing events recognized in the Collahuasi District, supporting a genetic link between the western intrusive bodies and the regional metallogenic framework.

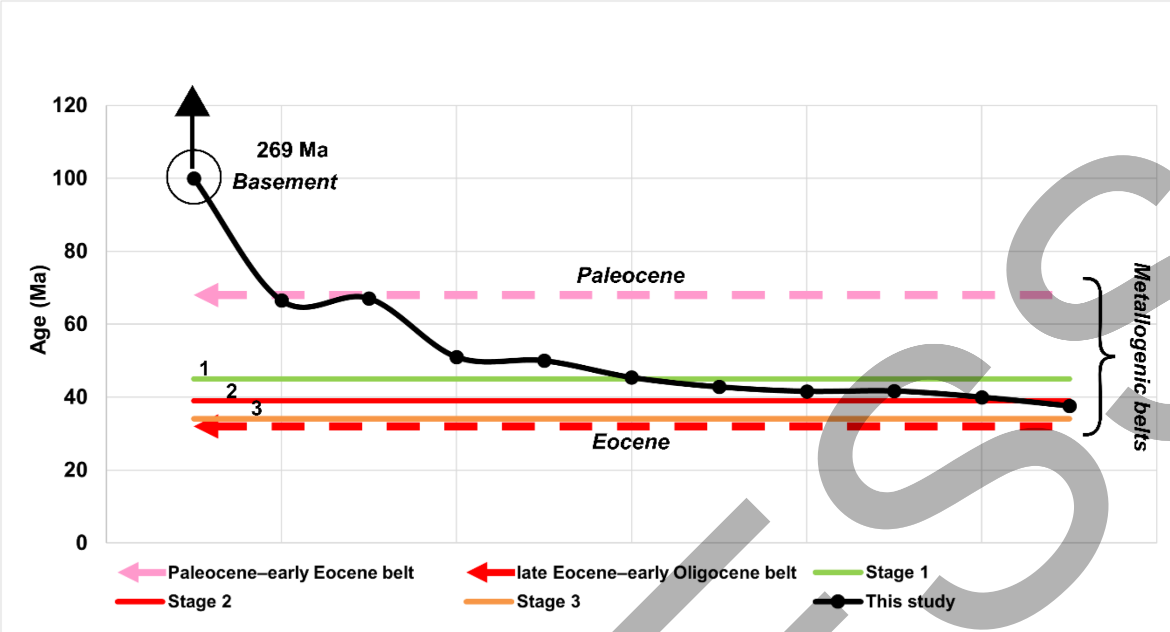

Fig. 10. Summary of the temporal relationship between the magmatic pulses identified in this study and the main metallogenic stages of the Paleocene-early Eocene and late Eocene-early Oligocene belts, showing that the Paleocene-Eocene intrusions emplaced west of the West Fault overlap with the early (Stage 1) to intermediate (Stage 2) mineralizing events of the Collahuasi District.

6 Conclusion

The new magmatic zircon ages obtained in this study allow for a more precise delineation of the magmatic evolution in the western sector of the Collahuasi District, revealing a complex intrusive history spanning from the late Permian to the late middle Eocene. The Maastrichtian-Bartonian intrusives predate and overlap spatially with the Paleocene-early Eocene and late Eocene-early Oligocene metallogenic belts of the Central Andes, providing a broader temporal framework for the evolution of porphyry copper systems in the region. These two belts are superposed in the study area, and the new U-Pb ages broaden the regional magmatic record toward Late Cretaceous and older events and refine the timing of Eocene magmatism within the established metallogenic framework. This overlap reflects a protracted and episodic magmatic evolution, in which intrusive pulses of different ages coexist spatially, highlighting the long-lived nature of arc magmatism and its progressive reactivation along the western part of the Collahuasi District.

The presence of intrusive bodies belonging to the Collahuasi Formation, together with Upper Cretaceous and Eocene intrusions located west of the West Fault, supports a probable westward extension of the Collahuasi District beyond its traditionally recognized structural boundary, thereby broadening the inferred spatial extent of the metallogenic system. The compositional diversity, variable degrees of hydrothermal alteration, and spatial association of these intrusions with major tectonic structures indicate that the central Colcol and southern Chojas sectors warrant further studies, particularly to assess their potential relationship with the Paleogene magmatic and metallogenic evolution of the Collahuasi District.

Acknowledgements

The authors would like to thank Compañía Minera Doña Inés de Collahuasi and Universidad Arturo Prat for their financial and logistical support during this study. The instrumentation at Macquarie University was funded by ARC LIEF and DEST Systemic Infrastructure Grants and enabled by NCRIS through AuScope. The authors also thank J. Piquer, A. Tomlinson, and an anonymous reviewer for their constructive comments and valuable contributions to the revision of this manuscript.

References

Aguilef, S.; Franco, C.; Tomlinson, A.J.; Blanco, N.; Álvarez, J.; Montecino, D.; Gardeweg, M.; Campos, V.; Rodríguez, C.; Maksaev, V.; Bodadilla, H.; Vásquez, P.; Grunder, A.L.; Dilles, J.H. 2019. Geología del área Quehuita-Chela, regiones de Tarapacá y Antofagasta. Servicio Nacional de Geología y Minería, Carta Geológica de Chile, Serie Geología Básica 207: 293 p., 1 mapa escala 1:100.000. Santiago.

Andersen, T. 2002. Correction of common lead in U–Pb analyses that do not report 204Pb. Chemical Geology 192(1–2): 59–79. https://doi.org/10.1016/S0009-2541(02)00195-X

AURUM Consultores. 2009. Estudio geológico-metalogénico Distrito Collahuasi. Informe Final Etapa II: Levantamiento geológico y metalogénesis a escala 1:50.000 y 1:25.000. Tomo I: Informe. Informe técnico preparado para Compañía Minera Doña Inés de Collahuasi, Servicios Geológicos y Mineros Ltda.–AURUM Consultores.

Berríos, M.; Maksaev, V. 2015. Geología y evolución tectónica del sistema de fallas Oeste–Domeyko en el segmento de Sierra Almeida, Región de Antofagasta, Chile. Revista Geológica de Chile 42(2): 231–255.

Black, L.P.; Gulson, B.L. 1978. The age of the Mud Tank Carbonatite, Strangways Range, Northern Territory. BMR Journal of Australian Geology and Geophysics 3: 227–232.

Black, L.P.; Kamo, S.L.; Allen, C.M.; Aleinikoff, J.N.; Davis, D.W.; Korsch, R.J.; Foudoulis, C. 2003. TEMORA 1: A new zircon standard for Phanerozoic U–Pb geochronology. Chemical Geology 200: 155–170. https://doi.org/10.1016/S0009-2541(03)00165-7

Blanco, N.; Tomlinson, A. 2013. Carta Guatacondo, Región de Tarapacá. Servicio Nacional de Geología y Minería, Carta Geológica de Chile, Serie Geología Básica 156: 109 p., 1 mapa escala 1:100.000. Santiago.

Boric, R.; Díaz, R.; Maksaev, V. 1990. Geología y yacimientos metalíferos de la Región de Antofagasta. Servicio Nacional de Geología y Minería, Boletín 40. Santiago.

Camus, F.; Castelli, J. 2021. Historia, Exploración y Geología de los Yacimientos Metalíferos de Chile 900–2020. Origo Publishing Co.: 1339 p. Santiago. ISBN 978-956-316-489-3.

Camus, F. 2005. The Andean porphyry systems. In: Porter, T.M. (ed.), Super Porphyry Copper & Gold Deposits: A Global Perspective. PGC Publishing, Adelaide, Vol. 1: 45–63.

Camus, F.; Dilles, H. 2001. A special issue devoted to porphyry copper deposits of Northern Chile. Economic Geology 96(2): 233–237.

Charrier, R.; Maksaev, V.; Elgueta, S.; Farías, M.; Morata, D.; Aguirre, L.; Muñoz, N. 2007. Evolución tectónica y magmática del margen andino de Chile y Argentina entre los 28° y

34°S. En: Hervé, F. (ed.), Geología de Chile. Servicio Nacional de Geología y Minería: 187–232. Santiago.

Clark, A.H.; Archibald, D.A.; Lee, A.W.; Farrar, E.; Hodgson, C.J. 1998. Laser probe 40Ar/39Ar ages of early- and late-stage alteration assemblages, Rosario porphyry copper-molybdenum deposit, Collahuasi district, I Region, Chile. Economic Geology 93: 326–337.

Damm, K.W.; Pichowiak, S.; Harmon, R.S.; Todt, W.; Kelley, S.; Omarini, R.; Niemeyer, H. 1990. Pre-Mesozoic evolution of the central Andes: the basement revisited. Special Paper of the Geological Society of America 241: 101–126.

Gain, S.E.M.; Gréau, Y.; Henry, H.; Belousova, E.; Dainis, I.; Griffin, W.L.; O'Reilly, S.Y. 2019. Mud Tank Zircon: Long-term evaluation of a reference material for U-Pb dating, Hf-isotope analysis and trace element analysis. Geostandards and Geoanalytical Research 43: 339–354. https://doi.org/10.1111/ggr.12265

García, M.; Maksaev, V.; Townley, B.; Dilles, J.H. 2017. Metallogeny, structural evolution, post-mineral cover distribution and exploration in concealed areas of the northern Chilean Andes. Ore Geology Reviews 86: 652–672. https://doi.org/10.1016/j.oregeorev.2017.01.025

Griffin, W.L. 2008. GLITTER: data reduction software for laser ablation ICP-MS. En: Sylvester, P.J. (ed.), Laser Ablation ICP-MS in Earth Sciences: Current Practices and Outstanding Issues. Mineralogical Association of Canada Short Course Series 40: 308–311. ISBN 9-0-921294-49-8.

Ireland, T. 2009. Permo-Triassic extension and the localization of Paleogene porphyry Cu deposits in the Collahuasi district. XII Congreso Geológico Chileno, Actas 12: S11_017, 4 p. Santiago.

Ireland, T. 2010. Geological framework of the mineral deposits of the Collahuasi district, Región de Tarapacá, Chile. Ph.D. Thesis, University of Tasmania: 460 p. Hobart, Australia.

Jackson, S.E.; Pearson, N.J.; Griffin, W.L.; Belousova, E.A. 2004. The application of laser ablation-inductively coupled plasma-mass spectrometry to in situ U–Pb zircon geochronology. Chemical Geology 211(1–2): 47–69. https://doi.org/10.1016/j.chemgeo.2004.06.017

Kay, S.M.; Mpodozis, C. 2001. Central Andean ore deposits linked to evolving shallow subduction systems and thickening crust. Geological Society of America Memoirs 204: 21–59. https://doi.org/10.1130/0-8137-1204-3.21

Ludwig, K.R. 2009. User's Manual for Isoplot 3.70. A Geochronological Toolkit for Microsoft Excel. Berkeley Geochronology Center, Special Publication 4.

Maksaev, V.; Munizaga, F.; Mathur, R.; Barra, F.; Fanning, C.M.; McWilliams, M.; Ruiz, J.; Sanhueza, A. 2009. Geochronology of the Collahuasi porphyry Cu-Mo district, north Chilean Andes. XII Congreso Geológico Chileno, Abstract S11_021, 4 p.

Maksaev, V.; Munizaga, F.; Tornos, F.; Palacios, C.; Steltenpohl, D. 2007. Geología y evolución del distrito pórfido de cobre Quebrada Blanca, Región de Tarapacá, Chile. Revista Geológica de Chile 34(1): 19–48. https://doi.org/10.4067/S0716-02082007000100002

Maksaev, V. 1990. Metallogeny, Geological Evolution, and Thermochronology of the Chilean Andes between latitudes 21° and 26° South, and the Origin of Major Porphyry Copper Deposits. Ph.D. Thesis, Dalhousie University, Nova Scotia, Canada: 497 p.

Maksaev, V.; Zentilli, M. 1988. Marco metalogénico regional de los depósitos de tipo pórfido cuprífero del Norte Grande de Chile. In Congreso Geológico Chileno, No. 5, Tomo I: B181–B212.

Masterman, G.J.; Cooke, D.R.; Berry, R.F.; Clark, A.H.; Archibald, D.A.; Mathur, R.; Walshe, J.L.; Durán, M. 2004. 40Ar/39Ar and Re-Os geochronology of porphyry copper-molybdenum deposits and related copper-silver veins in the Collahuasi district, northern Chile. Economic Geology 99(4): 673–690. https://doi.org/10.2113/gsecongeo.99.4.673

Mpodozis, C.; Cornejo, P. 2012. Cinturones metalogénicos de Chile: Actualización y perspectivas para la exploración de recursos minerales. Sociedad Nacional de Minería (SONAMI): 36 p. Santiago.

Mpodozis, C.; Ramos, V.A. 1990. The Andes of Chile and Argentina. En: Ericksen, G.E.; Cañas Pinochet, M.T.; Reinemund, J.A. (eds.), Geology of the Andes and its Relation to Hydrocarbon and Mineral Resources. Circum-Pacific Council for Energy and Mineral Resources, Earth Science Series 11: 59–90.

Münchmeyer, C.; Hunt, J.P.; Ware, H. 1984. Geología del distrito de Collahuasi y del pórfido cuprífero Rosario. Reporte Interno (Inédito), Compañía Minera Doña Inés de Collahuasi: 84 p. Santiago.

Munizaga, F.; Maksaev, V.; Fanning, C.M.; Giglio, S.; Yaxley, G.; Tassinari, C.C.G. 2008. Late Paleozoic–Early Triassic magmatism on the western margin of Gondwana: Collahuasi area, Northern Chile. Gondwana Research 13(3): 407–427. https://doi.org/10.1016/j.gr.2007.12.005

Richards, J.P. 2003. Tectono-magmatic precursors for porphyry Cu-(Mo-Au) deposit formation. Economic Geology 98(8): 1515–1533. https://doi.org/10.2113/gsecongeo.98.8.1515

Scheuber, E.; Bogdanic, T.; Jensen, A.; Reutter, K.J. 1994. Tectonic development of the North Chilean Andes in relation to plate convergence and magmatism since the Jurassic. In: Reutter, K.J.; Scheuber, E.; Wigger, P.J. (eds.), Tectonics of the Southern Central Andes. Springer-Verlag: 121–139.

Scheuber, E.; Andriessen, P.A.M. 1990. The kinematic and geodynamic significance of the Atacama Fault Zone, northern Chile. Journal of Structural Geology 12(2): 243–257. https://doi.org/10.1016/0191-8141(90)90008-M

Sillitoe, R.H.; Perelló, J. 2005. Andean copper province: Tectonomagmatic settings, deposit types, metallogeny, exploration, and discovery. En: Hedenquist, J.W. et al. (eds.), Economic Geology 100th Anniversary Volume, Society of Economic Geologists: 845–890.

Sillitoe, R.H. 2010. Porphyry copper systems. Economic Geology 105(1): 3–41. https://doi.org/10.2113/gsecongeo.105.1.3

Sillitoe, R.H.; Perelló, J. 2024. Porphyry copper recurrence in the Andes of Chile and Argentina. Economic Geology 119(5): 995–1003. https://doi.org/10.5382/econgeo.5092

Spencer, C.; Kirkland, C.; Taylor, R. 2016. Strategies towards statistically robust interpretations of in situ U-Pb zircon geochronology. Geoscience Frontiers 7(4): 581–589. https://doi.org/10.1016/j.gsf.2015.11.006

Tera, F.; Wasserburg, G.J. 1972. U-Th-Pb systematics in three Apollo 14 basalts and the problem of initial Pb in lunar rocks. Earth and Planetary Science Letters 14(3): 281–304. https://doi.org/10.1016/0012-821X(72)90128-8

Tomlinson, A.J.; Blanco, N.; Maksaev, V.; Dilles, J.H.; Grunder, A.; Ladino, M. 2001. Geología de la Precordillera Andina de Quebrada Blanca–Chuquicamata, Regiones I y II (20º30'–22º30'S). Servicio Nacional de Geología y Minería, Informe Registrado IR-01-20: 444 p., 20 mapas escala 1:50.000. Santiago.

Vergara, H. 1978. Cuadrángulo Quehuita y sector occidental del cuadrángulo volcán Miño, Región de Tarapacá. Instituto de Investigaciones Geológicas, Carta Geológica de Chile Nº 32, mapa escala 1:50.000, 44 p. Santiago.

Vergara, H.; Thomas, A. 1984. Hoja Collacagua: Región de Tarapacá. Servicio Nacional de Geología y Minería, Carta Geológica de Chile 59, escala 1:250.000. Santiago. Disponible en: www.sernageomin.cl

Vermeesch, P. 2018. IsoplotR: A free and open toolbox for geochronology. Geoscience Frontiers 9(5): 1479–1493. https://doi.org/10.1016/j.gsf.2018.04.001

Wiedenbeck, M.; Alle, P.; Corfu, F.Y.; Griffin, W.L.; Meier, M.; Oberli, F.V.; Quadt, A.V.; Roddick, J.C.; Spiegel, W. 1995. Three natural zircon standards for U-Th-Pb, Lu-Hf, trace element and REE analyses. Geostandards Newsletter 19: 1–23. https://doi.org/10.1111/j.1751-908X.1995.tb00147.x

Williams, W.C. 1992. Magmatic and structural controls on mineralization in the Paleocene magmatic arc between 22°40′ and 23°45′ South Latitude, Antofagasta, II Region, Chile. Ph.D. Thesis, The University of Arizona: 182 p. Tucson, Arizona, USA.